Erosion Prediction in Ungauged Basins: Integrating Methods and Techniques (Proceedings of symposium HS01 held during IUGG2003 at Sapporo, July 2003). IAHS Publ. no. 279, 2003.

Effects of land-use change on runoff response in the ungauged Ta-Chou basin, Taiwan

PAO-SHAN YU, YU-CHI WANG & CHUN-CHAO KUO

Department of Hydraulic and Ocean Engineering, National Cheng Kung University, Tainan 70101, Taiwan

yups@mail.ncku.edu.tw

Abstract Land development and urbanization have increased significantly in Taiwan over the last two decades because of the increasing population and economic development. The ungauged Ta-Chou basin, which is representative of drainage basins undergoing these changes, was chosen to investigate the effects of land-use change on surface runoff. Supervised classification of Landsat MSS and SPOT satellite images was used to show land-use change from 1972 to 2000. During this period, the area of impervious land increased by approximately 220%, and the area occupied by rice paddies decreased by about 55%. Results from a distributed rainfall–runoff model reveal that the observed land-use change causes increases in both peak discharge and total runoff. For design storms having return periods ranging from 10 to 200 years, peak discharge increased from 6 to 10% and total runoff increased from 10 to 17%. The methods outlined may be used to investigate the effects of land-use change on runoff response in ungauged basins elsewhere.

Key words geographic information systems; land-use change; rainfall–runoff model; remote sensing; Ta-Chou basin, Taiwan; ungauged basin

INTRODUCTION

Land development and urbanization in Taiwan have increased substantially over the last two decades. The change of land-use type has had a considerable impact on the nature of runoff and related hydrological characteristics. For example, evapo-transpiration and interception may decrease after trees and vegetation are removed in the process of urbanization. Later, an increase in impervious area due to the construction of houses, streets and culverts may reduce infiltration and shorten the time of concentration. Generally, urbanization will increase peak discharge and runoff volume (Weng, 2001). Unfortunately, most areas are not suitably monitored to quantify such changes. Quantifying the effects of land-use change and urbanization on the hydrograph, therefore, frequently depends on distributed rainfall–runoff models that can simulate spatial hydrological processes.

Remote sensing (RS) techniques have been applied extensively and are recognized as powerful and effective tools for detecting land-use change. Recently, remote sensing and geographic information systems (GIS) have been integrated and applied with hydrological models. Remote sensing collects multi-spectral, multi-resolution, multi-temporal data, and turns them into useful information. GIS technology provides a flexible environment for entering, analysing, and displaying digital data from various sources, for identifying urban features, detecting change, and developing databases.

Data collected and treated by RS and GIS are used as inputs for models to simulate hydrological processes. Rango (1985) combined RS and a hydrological model, and showed that RS can obtain more complete data in wide areas to promote efficient simulation. Schultz (1988) utilized Landsat images to determine the input parameters for a watershed. Schumann (1993) applied GIS to manage and analyse spatial geographic input data, and established the parameters of a conceptual, semi-distributed model. Weng (2001) developed an integrated approach to combine RS and GIS techniques to elucidate the effects of urban growth on surface runoff using a simple Soil Conservation Service (SCS) model.

Taiwan has the same significant urbanization problem as other counties in the world. This study aims to investigate the effect of land-use change on runoff using a distributed rainfall–runoff model coupled with RS and GIS techniques.

STUDY AREA

The Ta-Chou basin (Fig. 1), a sub-basin of Yan-Shui basin in southern Taiwan, has a main channel length of 9.5 km and a drainage area of 35 km^2. The climate is sub-tropical, with a mean annual temperature of 24°C. Mean annual rainfall is approximately 1650 mm; 90% of all rainfall occurs during the wet period from May to October.

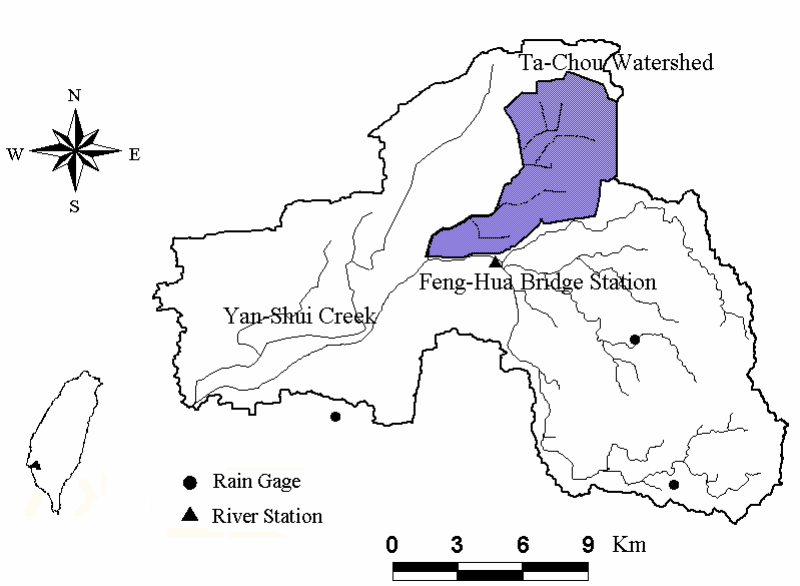

Fig. 1 Location of study area

METHODS

Land-use change detection

Normally, field investigations and aerial photographs are used to detect changes in land use. Field investigations, however, are inefficient and expensive, whereas aerial

photographs are usually not obtained in real time, and thus do not reflect the actual needs. Recently, satellite remote sensing has served as a useful tool to classify land use and to assess land-use change. In this study, satellite images are used to perform such classification and assessment.

The 1972 Landsat MSS and 2000 SPOT images are used to identify types of land-use using both traditional supervised and unsupervised classification methods, in which the maximum likelihood method and the ISODATA (Iterative Self-Organizing Data Analysis Technique) algorithm are applied separately. Ground-truth data at training sites are required before supervised classification can be conducted. Archival aerial photographs, acquired in 1972, were chosen to classify land use on the 1972 Landsat MSS images. No suitable aerial photographs were available for the year 2000. Consequently, ground truthing was carried out in the field to classify land use in the 2000 SPOT imagery. During the field investigations, the types of land use and corresponding geographic coordinates were recorded using a global positioning system (GPS).

ERDAS Imagine software was used for the land-use classification. The classifications by both supervised and unsupervised methods are compared with the ground truth in order to estimate their reliability. The classification results in Table 1 reveal that the supervised method provides a better assessment of the land-use patterns than the unsupervised method. Hence, the classification results of the supervised method have been adopted as the baseline information for further analysis in this study. Figure 2 displays the classified land-use types from the 1972 and 2000 satellite images obtained using the supervised method. The land-use types in Fig. 2 are compared to estimate land-use change between 1972 and 2000. The results in Table 2 indicate that land-use patterns have changed during this period. Most evident is the urban area; it shows an increase of about 220%. Simultaneously, the total area of water, dry farmland and rice paddies decreased by about 50%.

Table 1 Accuracy analysis of 1972 and 2000 images (%).

Class	1972		2000	
	Unsupervised accuracy	Supervised accuracy	Unsupervised accuracy	Supervised accuracy
Urban	50	50	40	92
Water	85	75	90	93
Dry farmland	50	85	70	97
Paddy	85	90	80	97
Total accuracy	68	75	70	95

Table 2 Land-use change in the Ta-Chou drainage basin.

Class	Area in 1972 (m^2)	Percentage of area (%)	Area in 2000 (m^2)	Percentage of area (%)	Change (%)
Urban	6 910 655	19.87	22 136 662	63.7	220.3
Water	1 399 423	4.02	721 139	2.1	–48.5
Dry farmland	19 588 996	56.33	8 821 057	25.3	–55.0
Paddy	6 878 316	19.78	3 098 543	8.9	–55.0

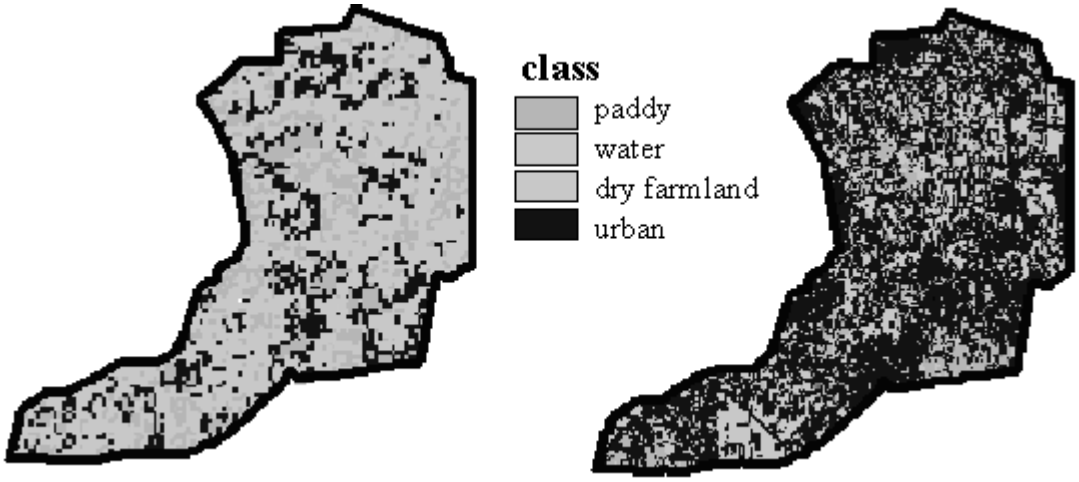

Fig. 2 Supervised classification of images for 1972 (left) and 2000 (right).

Runoff calculations

The influence of observed land-use changes on runoff is examined using a distributed rainfall–runoff model and design hyetographs with various return periods. The Ta-Chou drainage basin is divided into 0.5 × 0.5 km grid cells, for which slope, elevation, soil characteristics, vegetation type, ground cover, and overland flow direction are specified. The model is based on Horton overland flow (rainfall rate in excess of infiltration rate and ponding). The contributions of subsurface flow are ignored in this first-order runoff estimation technique. Infiltration is calculated with the Horton infiltration equation (Viessman *et al.,* 1989):

$$f_p(t) = f_c + (f_0 - f_c)\mathrm{e}^{-kt_r} \tag{1}$$

where $f_P(t)$ denotes infiltration capacity, f_C is initial infiltration capacity, f_0 is final infiltration capacity, k denotes the decay constant, and t_r is time. In reality, the infiltration rate is equal to the lesser of infiltration capacity and rainfall intensity. Thus, the study applies the adjusted form of the Horton infiltration equation (Viessman *et al.*, 1989) to estimate the infiltration rate. Each storm event has its own antecedent conditions and optimal initial infiltration capacity, so a calibrated parameter *Ch* is used here to obtain the optimal initial infiltration parameters (Yu & Jeng, 1997).

For overland flow, each grid is considered to be a conceptual reservoir. The drainage basin storage is calculated using a nonlinear storage approach, written as:

$$S = K_{SN}Q^m \tag{2}$$

where K_{SN} is the storage coefficient, Q is outflow, and S is storage.

The continuity equation for each grid cell is:

$$\frac{(I_t + I_{t+\Delta t})}{2} - \frac{(Q_t + Q_{t+\Delta t})}{2} = \frac{(S_{t+\Delta t} - S_t)}{\Delta t} \tag{3}$$

where Δt denotes calculation time step and I is inflow. In a grid with length L, width w and water depth y, S is calculated as:

$$S = ywL \tag{4}$$

Discharge, Q, is determined by Manning's equation:

$$Q = 1/n\, wy^{5/3} S_b^{1/2} \tag{5}$$

where n is the Manning coefficient, S_b is surface slope, and w and y are as above. Combining equations (4) and (5) yields:

$$S = n^{0.6} w^{0.4} L S_b^{-0.3} Q^{0.6} \tag{6}$$

which is the same form as equation (2) with:

$$m = 0.6 \tag{7}$$

and

$$K_{SN} = n^{0.6} w^{0.4} L S_b^{-0.3} \tag{8}$$

The discharge at $t + \Delta t$ is estimated iteratively using the Newton-Raphson method to solve the continuity equation (3):

$$Q'_{t+\Delta t} = Q_{t+\Delta t} - \frac{\Delta t(Q_{t+\Delta t} + Q_t - I_{t+\Delta t} - I_t) + 2K_{SN}(Q^m_{t+\Delta t} - Q^m_t)}{\Delta t + 2K_{SN} m Q^{m-1}_{t+\Delta t}} \tag{9}$$

The inflow I in equation (9) includes rainfall and lateral flow from up to four neighbouring grid cells; hence, the inflow I_t can be represented as:

$$I_t = R_t + \sum_{j=1}^{4} Q_j(t' + L_t) - f_t \tag{10}$$

where R_t is rainfall, j is the number of the neighbouring grid cell, L_t is the lag time of overland flow from neighbouring cells, $Q_j(t' + L_t)$ denotes the inflow at time step t from a neighbouring cell, which is the lateral outflow of the neighbouring grid cell at time t' plus the lag time L_t so that ($t' + L_t = t$), and f_t is the infiltration.

The channel flow is calculated in a manner similar to that of overland flow discussed above. Each channel section is treated as a conceptual reservoir, for which the channel storage coefficient K_{CN} is written as:

$$K_{CN} = n_c^{0.6} w_c^{0.4} L_c S_c^{-0.3} \tag{11}$$

where n_c is the Manning coefficient of the channel, S_c is the channel slope, w_c is the channel width, and L_c is the channel length that depends on the grid size. As the values of n, n_c, S_b and S_c may involve uncertainty, the lumped parameters Cs and Cc are introduced to adjust the storage coefficients K_{SN} and K_{CN}.

Model calibration

The parameters in the distributed rainfall–runoff model are divided into two types: physical parameters (i.e. model input data), which can be generated directly from

topographic, soil, and vegetation maps; and calibrated parameters, which are derived from historical rainfall and flow data. The three calibration parameters (*Ch*, *Cs*, and *Cc*) in the model are calibrated by applying both the Shuffled Complex Evolution (SCE) (Duan *et al.*, 1992) optimization technique and an objective function. The SCE method is a general-purpose, global optimization strategy designed to solve the various response surface problems encountered in calibrating a nonlinear simulation model. Detailed explanations of the method appear in Duan *et al.* (1992, 1993, 1994).

RESULTS

Model validation

As no observed runoff data from the study area (Ta-Chou basin) are available, the model parameters are calibrated using data from a neighbouring basin (Feng-Hua Bridge station). The characteristics of the flood hydrographs chosen for model calibration and verification are given in Table 3. The maximum error of the time to peak is smaller than two hours, the average error of the peak discharge is 6%, and the average total volume error is approximately 16%, with an average coefficient of efficiency (Nash & Sutcliffe, 1970) of 0.89. The model thus seems to provide reasonable results. Accordingly, the average parameters (*Cs* = 0.482, *Cc* = 0.578, *Ch* = 0.053) in Table 3 were used for model verification. The verification results in Table 4

Table 3 Optimal parameter sets and performances for storm events used for calibration.

Storm event	*Cs*	*Cc*	*Ch*	ETP (h)	EQP (%)	VER (%)	CE	OBJ
Event 1	0.024	0.559	0.021	1	4.25	–18.29	0.96	40.29
Event 3	0.018	0.730	0.014	–1	–13.91	–27.04	0.90	41.31
Event 4	0.024	1.240	0.013	0	0.48	–16.39	0.88	19.48
Event 5	0.647	0.658	0.094	1	–1.28	–6.07	0.97	8.95
Event 6	0.020	0.520	0.024	0	–2.63	–30.72	0.89	46.11
Event 7	0.021	0.707	0.015	4	–15.33	–23.64	0.79	33.86
Event 8	0.503	0.522	0.260	–1	–1.59	–3.12	0.97	8.96
Event 9	0.041	0.725	0.132		5.52	–11.35	0.97	22.39
Event 10	0.012	0.473	0.011	–2	–3.53	–20.26	0.76	77.84
Event 11	0.015	0.519	0.027	–1	–1.95	–25.79	0.77	50.46
Event 12	2.059	0.153	0.012	–2	16.11	–5.79	0.91	29.62
Event 13	2.396	0.131	0.012	–3	5.54	0.76	0.86	24.09
Average	0.482	0.578	0.053	1.3	6.01	15.77	0.89	62.06

Table 4 Performances for storm events used for verification.

Storm event	ETP (h)	EQP (%)	VER (%)	CE
Event 2	1	4.78	–26.81	0.72
Event 14	–1	–20.09	–27.32	0.71
Event 15	0	–22.64	–35.45	0.78
Event 16	–1	–8.15	–29.17	0.80
Event 17	1	–6.21	–29.60	0.72
Average	0.8	12.37	29.67	0.75

show that the average error of the time to peak is around 0.8 h, the average error of the peak discharge is less than 13%, the average error of total volume is about 30%, and the average coefficient of efficiency is 0.75.

The impact of land-use change on runoff

Twenty-four hour design hyetographs for various return periods were developed based on the Alternating Block method and IDF formulas, which are generated using a Pearson type III distribution. The hydrographs for various return periods can be obtained by using the 24-hour design hyetographs in the distributed rainfall–runoff model. The effect of land-use changes on runoff can then be evaluated. The hydrographs for various return periods are estimated by running the distributed rainfall–runoff model with the 1972 and 2000 land-use scenarios. The results indicate that peak discharge and runoff volume increase significantly from 1972 to 2000 (Table 5).

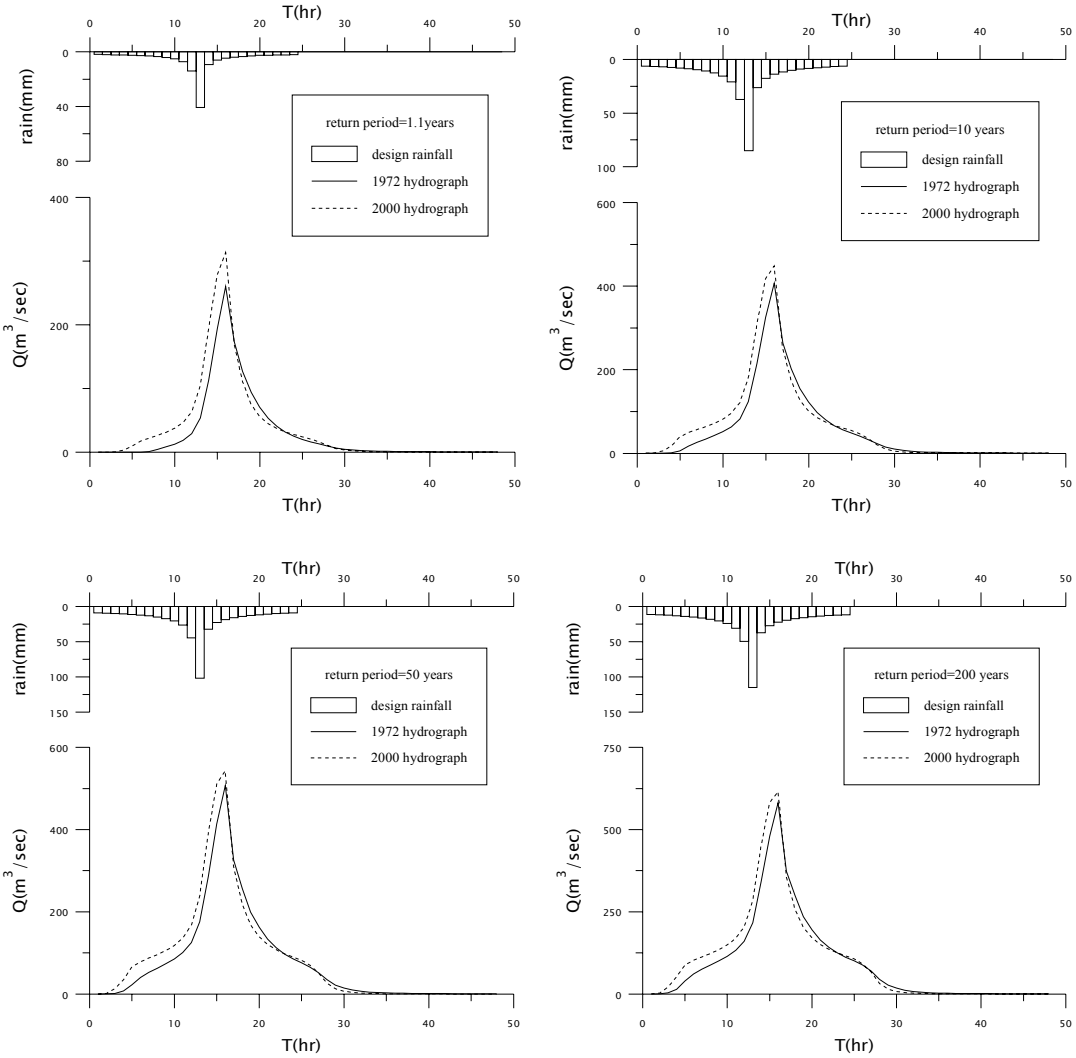

Fig. 3 Hydrographs for various return periods with different land-use scenarios.

Table 5 Impact of land-use change on runoff in the Ta-Chou basin.

Return period (years)	1972 Peak discharge ($m^3 s^{-1}$)	Runoff volume (m^3)	2000 Peak discharge ($m^3 s^{-1}$)	Runoff volume (m^3)	Change Peak discharge (%)	Runoff volume (%)
1.1	137	2 283 824	196	3 356 993	43.1	47.0
2	260	5 024 041	313	6 431 105	20.4	28.0
5	352	7 675 081	398	9 239 485	13.1	20.4
10	407	9 462 581	449	11 064 500	10.3	16.9
25	466	11 546 910	504	13 206 680	8.2	14.4
50	508	13 048 210	543	14 738 370	6.9	13.0
100	546	14 516 960	579	16 246 620	6.0	11.9
200	581	15 988 990	615	17 760 310	5.9	11.1

Figure 3 and Table 5 show that the increase in peak discharge and runoff volume between 1972 and 2000 becomes smaller for longer return periods. This can be attributed to the increase in impervious area, since this has been documented as the major change in land use. The increase in impervious area causes a decrease in infiltration capacity, which has a greater effect on runoff for shorter return periods.

CONCLUSIONS

The influence of land-use change on hydrological processes is not effectively monitored. Studying the effects of land-use change on runoff therefore requires a distributed rainfall–runoff model. This study combines remote sensing and GIS techniques to provide the topographical and land-use data for a grid-based, distributed rainfall–runoff model that is used to assess the impact of land-use change on runoff. The extent of urban areas in the Ta-Chou study basin increased by approximately 220% from 1972 to 2000, based on image analysis for those two years. Simulations of stream flow show that the peak discharge and runoff volume for 10-year return period design rainfall increased by 10 and 17%, respectively. The results also reveal that land-use change caused by humans may increase the probability of flooding and damage.

Acknowledgements The authors would like to thank to the National Science Council, Republic of China, for financial support under grant no. NSC90-2625-Z-006-001.

REFERENCES

Duan, Q., Sorooshian, S. & Gupta, V. K. (1992) Effective and efficient global optimization for conceptual rainfall–runoff models. *Wat. Resour. Res.* **28**(4), 1015–1031.

Duan, Q., Gupta, V. K. & Sorooshian, S. (1993) A shuffled complex evolution approach for effective and efficient global minimization. *J. Optimization Theory Appl.* **76**(3), 501–521.

Duan, Q., Sorooshian, S. & Gupta, V. K. (1994) Optimal use of the SCE-UA global optimization method for calibrating watershed models. *J. Hydrol*. **158**, 265–284.

Nash, J. E. & Sutcliffe, V. (1970) River flow forecasting through conceptual models. I. A discussion of principles. *J. Hydrol.* **10**, 282–290.

Rango, A. (1985) Assessment of remote sensing input to hydrologic model. *Wat. Resour. Bull.* **21**(3), 423–432.

Schultz, A. G. (1988) Remote sensing in hydrology. *J. Hydrol.* **100**, 239–265.

Schumann, A. H. (1993) Development of conceptual semi-distributed hydrological models and estimation of their parameters with the aid of GIS. *Hydrol. Sci. J.* **38**(6), 519–528.

Viessman, W. Jr, Lewis, G. L. & Knapp, J. W. (1989) *Introduction to Hydrology.* Harper and Row, New York, USA.

Weng, Q. (2001) Modeling urban growth effects on surface runoff with the integration of remote sensing and GIS. *Environ. Manage.* **28**(6), 737–748.

Yu, P. S. & Jeng, Y. C. (1997) A study on grid based distributed rainfall runoff models. *Wat. Resour. Manage.* **11**, 83–99.